Article

Design of Shiitake Mushroom Robotic Picking Grasper: Considering Stipe Compressive Stress Relaxation

Jianxun Li [1,2], Qingchun Feng [2,3] , Mengfei Ru [2,3], Jiahui Sun [2,3], Xin Guo [2,3] and Wengang Zheng [2,*]

1 College of Mechanical Engineering, Guangxi University, Nanning 530004, China; 15195936828@163.com
2 Intelligent Equipment Research Center, Beijing Academy of Agriculture and Forestry Sciences, Beijing 100097, China; fengqc@nercita.org.cn (Q.F.); rumengfei1993@163.com (M.R.); sjiahui9@126.com (J.S.); guoxin@nercita.org.cn (X.G.)
3 Beijing Key Laboratory of Intelligent Technology for Agriculture, Beijing 100097, China
* Correspondence: zhengwg@nercita.org.cn

Abstract: In order to realize the automatic picking of shiitake mushrooms and reduce the risk of damage to shiitake mushrooms in the picking process, this paper designed a shiitake mushroom picking grasper. First, this paper carries out mechanical tests of compression and stress relaxation on sections of shiitake mushroom stipes, and establishes the component stress relaxation equations of shiitake mushroom stipes. The compression mechanical characteristics of the entire mushroom stipe are then analyzed using finite element analysis, with a mean square error of less than 5% compared to actual results. Second, based on the actual picking experience, this paper proposes an "L"-shaped three-finger picking grasper, and analyzes the mechanical relationship between the grasper's gripping force, twisting separation torque, and servo output torque. Furthermore, according to the mechanical constitutive model of mushroom stipes, the optimal twisting separation torque and corresponding servo motor output torque for the grasper are determined. The picking grasper designed in this paper was tested for picking mushrooms of different growth periods, and the test results show that the picking grasper designed in this paper is able to grasp and separate the mushrooms quickly and without damage.

Keywords: mushroom picking; picking grasper; stress relaxation; finite element analysis

1. Introduction

The shiitake mushroom is one of the edible fungi with the largest cultivation scale and cultivation range in the world due to its good edible and medicinal values [1]. China's shiitake mushroom production ranks first in the world, accounting for over 90% of the global production, which reached 12.554 million tons in 2021 [2]. Shiitake mushrooms cultivated in sticks require selective and timely harvesting at high frequency to ensure their perfect edible quality. Currently, relying on manual picking consumes a large amount of labor and becomes an important factor in increasing production costs [3]. Consequently, there is growing interest in China's development of autonomous harvesting robots to replace manual labor.

During the harvesting process, conducting non-destructive operations on the tender fruit bodies of shiitake mushrooms is a prerequisite for achieving mechanized harvesting [4–6]. Shiitake mushroom fruit bodies consist of a cap and a stipe. The traditional manual picking method involves gripping the base of the stipe with the thumb and index finger of one hand, rotating the stipe left and right, and slowly pulling it upward to detach it from the substrate. When harvesting, it should also be noted that the hand can only touch the stipe, and cannot bruise the cap and folds. If the method of root excision is adopted, it may lead to stipe residues remaining on the mushroom stick, affecting future mushroom growth. Therefore, according to the manual harvesting skills, the mushroom stipe needs

to be reliably and safely gripped, ensuring sufficient force for picking while avoiding any damage to the stipe.

The quality and efficiency of shiitake mushroom harvesting are directly determined by the picking grasper, making it a crucial component of robot harvesting systems. Currently, both domestic and international scholars have conducted extensive research on end effectors for harvesting umbrella-shaped edible fungi. Catha and Van et al. developed mushroom harvesting machines that utilize blades for mushroom harvesting. However, rigid blade harvesting severely damaged mushroom quality, rendering it suitable only for processed products. Reed et al. [7] developed a mushroom harvesting robot that utilizes vacuum suction cups made of corrugated tube silicone to grip the mushroom cap and twist it. Huang et al. [8] designed a picking grasper that also uses vacuum suction cups to grip the mushroom cap and utilizes a curved track to bend the mushroom. Lu Wei et al. [9] designed a flexible grasper with 3–4 joints, using a top-down twisting method for harvesting. Cheng et al. [10] designed a grasper for harvesting Agaricus bisporus mushrooms, which features a cylinder and an elastic sleeve structure, achieving harvesting through the contraction of liquid plastic in the elastic sleeve. The aforementioned graspers all exert force on the mushroom cap, but shiitake mushroom caps are soft and vulnerable, so touching them should be avoided. None of the aforementioned graspers meet the requirements for shiitake mushroom harvesting. Therefore, designing a picking grasper suitable for shiitake mushroom harvesting is necessary.

Currently, picking graspers for tender agricultural products are mainly categorized in two ways to achieve lossless gripping: active compliance and passive compliance. Active compliance is generally realized based on the feedback control of force, and its goal is to establish a desired dynamic relationship between the position of the robot's picking grasper and the environmental contact force [11]. On the other hand, passive compliance relies on the deformation of flexible components within the picking grasper to accomplish all the motions, thus realizing the transfer of force or energy. The application of flexible components allows for constant force output within a certain range, reducing the need for force sensing and control in constant force mechanisms [12]. Regardless of the compliance method used, the mechanical properties of the stipe itself when subjected to compression should be considered in order to realize compliant gripping of the stipe.

The stipe is a biologically characterized material with significant viscoelastic properties, which are manifested by the presence of dynamic relaxation of the extrusion stresses during the extrusion process, i.e., stress relaxation. Stress relaxation refers to the phenomenon where stress within a material gradually decays over time under constant temperature and deformation conditions [13]. Therefore, when the picking grasper grips the mushroom stipe for picking, it needs to consider the attenuation of the gripping force due to its stress relaxation, to ensure that the grasper can maintain sufficient gripping force on the mushroom stipe during the picking process, so that it does not fall off and cause picking failure. In order to quantitatively characterize the dynamic stress relaxation characteristics of materials, classical linear models such as Maxwell [14] and Burgers [15] are commonly used for fitting. Jiang et al. [16] investigated the stress relaxation characteristics of the lychee and described it with the Maxwell model, achieving a high coefficient of determination (R^2) of 0.998, indicating a high fitting accuracy. Xia et al. [17] quantified the stress relaxation characteristics of the carrot by using the Maxwell model in order to analyze the impact damage of the carrot. Zou et al. [18] investigated the stress relaxation characteristics of green leafy vegetables, focusing on spinach as a representative vegetable, and derived the stress relaxation characteristics under gripping conditions using the Burgers model. Therefore, the classical linear model such as Maxwell is suitable for fitting the stress dynamic relaxation characteristics of fruits and vegetables.

In this paper, for the demand of mechanized mushroom harvesting, drawing on manual picking operation skills, a new type of shiitake mushroom picking grasper with integrated stipe gripping and twisting is designed. Additionally, the compressive stress relaxation model of mushroom stipe is established to determine the optimal gripping force

of the picking grasper, thereby enhancing the reliability of harvesting. As a key component of mushroom picking machinery, this study can promote the development and application of mushroom picking robots.

2. Modeling of Compressive Stress Relaxation Characteristics of Mushroom Stipes

2.1. Materials

Currently, wood-rotted fungus sticks are mainly used to cultivate shiitake mushrooms, as shown in Figure 1. A selection of fresh shiitake mushrooms to be harvested were selected, characterized by no deformation, cracks, and damages. The relevant dimensions of cap and stipe were then measured, including cap height, cap diameter, stipe height, and stipe diameter, as shown in Figure 2. The basic parameters of the cap and stipe are summarized in Table 1, which serves as a basis for the subsequent design of the picking grasper.
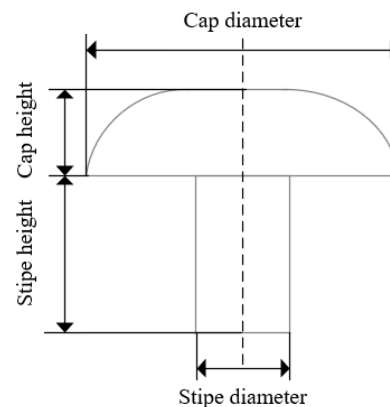

Figure 1. Shiitake mushrooms growing on sticks.

Figure 2. Cap diameter, cap height, stipe diameter, and stipe height measurement of mushrooms.

Table 1. Basic parameters of mushrooms. Values are means ± standard deviation.

Parameters	Values (mm)
Cap diameter	62 ± 12.2
Cap height	21.1 ± 4.2
Stipe diameter	13.2 ± 2.6
Stipe height	32.6 ± 5.5

The model can be simplified to a cylinder by removing the cap part of the mushroom and keeping only the stipe part. According to the direction of force, it can be divided into axial and radial directions. When actually picking, the mushroom stipe is twisted in the radial direction. Therefore, in this test, the main focus lies in the radial compression

mechanical properties of the mushroom stipe, with the compression test conducted along the radial direction of the mushroom stipe. In view of the different irregular shapes of individual shiitake mushrooms, it is difficult to estimate accurately the force area of the whole of them as a compression test sample, making the stresses impossible to calculate. Therefore, it is necessary to make a standard square sample of the mushroom stipe. The dimensions of the samples were 10 mm × 10 mm × 10 mm with an error of ±0.05 mm, totaling 100 square samples.

2.2. Compression Test

In order to determine the mechanical properties of the stipe, such as elastic modulus, Poisson's ratio, and biological yield point, compression tests were required for the stipe samples. The tests were carried out using the SMS texture analyzer from the UK, as shown in Figure 3. Room temperature conditions (22 °C ± 1 °C, 40–60% RH). The mushroom stipe sample was placed between the texture analyzer probe and the metal plate. The probe applied compression to the samples at a rate of 1 mm/s along the downward direction (within the quasi-static range). Each test included 10 samples.


1.probe 2. Sample 3. metal plate
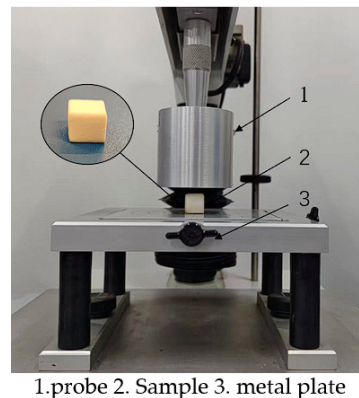
Figure 3. Compression test system.

The stress–strain curve of the mushroom stipe is obtained by the compression test, as shown in Figure 4. Before point A, the sample is in the elastic stage, where the curve is approximately linear, and the elastic modulus is the tangent line of the elastic stage. Point B is the yield point, and the yield stress is the stress at this point. When the curve reaches point B, the sample begins plastic deformation, and this deformation causes irreversible damage to the stipe. Point C is the failure point, and when the curve reaches point C, the sample ruptures and the stress begins to decrease. The deformation of stipe samples at points A, B, C is shown in Figure 5.
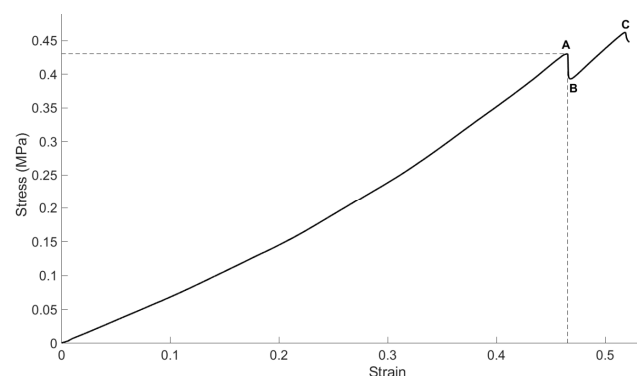
Figure 4. The stress–strain curve of stipe sample. A is the elastic limit, B is the yield point, C is the failure point.

(A) (B) (C)
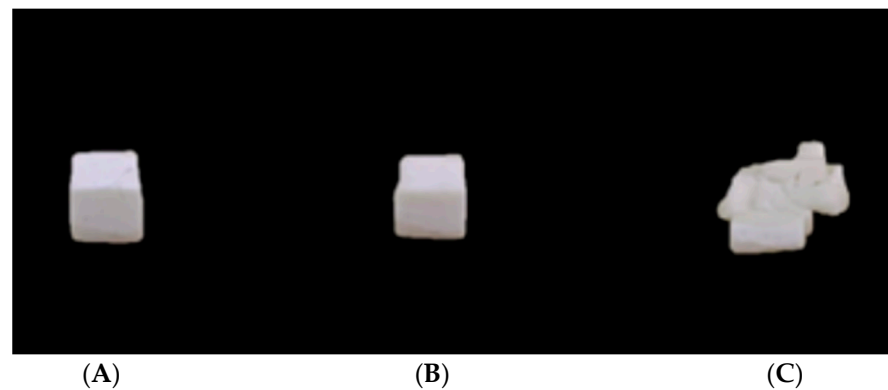
Figure 5. Deformation of stipe samples at points (**A**–**C**).

According to Equation (1), Poisson's ratio is calculated by measuring the ratio of the transverse positive strain to the radial positive strain of the sample:

$$\mu = \frac{\varepsilon_0}{\varepsilon_1} = \frac{\Delta L / L_0}{\Delta D / D_0} \tag{1}$$

In the equation, L_0 is the initial radial length before compression, i.e., side length 10 mm; ΔL is the deformation of radial length after compression; D_0 is the initial axial length before compression, i.e., side length 10 mm; ΔD is the deformation of axial length after compression.

Based on the stress–strain measurements of 10 groups of standard samples of mushroom stipes, their elastic-plastic parameters were calculated, and the average values of three parameters, namely elastic modulus, yield stress, and Poisson's ratio are shown in Table 2.

Table 2. Average value of stipe elastic-plastic material parameters.

Materials	Elastic Modulus (Mpa)	Bio-Yield Stress (Mpa)	Poisson's Ratio ($-$)
Stipe	0.871	0.418	0.322

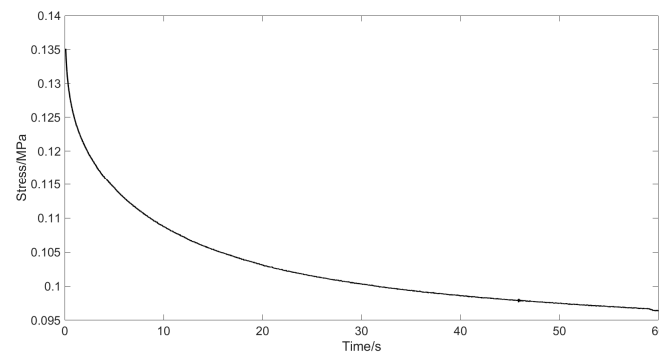*2.3. Stress Relaxation Test*

In order to quantitatively describe the stress relaxation characteristics of mushroom stipes, the relevant stress relaxation parameters of the stipes were obtained by stress relaxation tests to clarify the gripping dynamic decay law. For stress relaxation tests, an initial compressive stress needs to be applied. If the deformation of the stipe is too small, it cannot reflect the significant observed stress changes, while excessive deformation may lead to stipe damage [19]. According to the compression characteristics obtained in Section 2.2, we set the initial state of the relaxation test with a compression deformation of 2 mm (strain approximately 0.2, within the normal range of strain), and a pre-compression rate of 1 mm/s (within the quasi-static range). After the probe reached the initial state of compression, the displacement was kept unchanged for 60 s. The stress relaxation curve obtained dynamically by the texture analyzer is shown in Figure 6.

In order to solve the stress relaxation phenomenon of mushroom stipes, this study selected five elements of the generalized Maxwell model to fit the stress relaxation curve. The equation is shown in Equation (2), as follows:

$$E(t) = E_{1}e^{-t/T_1} + E_{2}e^{-t/T_2} + E_\infty \tag{2}$$

where $E(t)$ [Mpa] is the instantaneous modulus of elasticity at any time t; E_1 and E_2 is the decay elastic modulus; E_∞ [Mpa] is the equilibrium elastic modulus; T_1 and T_2 are the relaxation times of the Maxwell elements.

Figure 6. The stress relaxation curve of stipe.

According to the principle of least squares, the stress relaxation curves of the stipe samples were fitted using the successive approximation method. The fitting coefficient R^2 is 0.992, so the Maxwell model can be used to characterize the stress relaxation of the stipe. The final stress relaxation model for the stipe samples is shown in Equation (3), as follows:

$$E(t) = 0.02516e^{-t/2.7445} + 0.03088e^{-t/27.15} + 0.26195 \tag{3}$$

where $E_1 = 0.02516$, $E_2 = 0.03088$, $T_1 = 2.7445$, $T_2 = 27.15$, $E_\infty = 0.26195$.

2.4. Finite Element Analysis of Stress Relaxation

2.4.1. Finite Element Modeling

With the mechanical compression properties and stress relaxation characteristics of the standard samples obtained, ABAQUS finite element modeling was employed to analyze quantitatively the viscoelastic properties of variously shaped whole shiitake mushroom stipes. The stress relaxation tests of the mushroom stipes were simulated. The simulation conditions were the same as the actual experimental conditions; the metal plate was fixed, and the mushroom stipes were compressed by the texture analyzer probe along the downward direction.

In the material attribute module, the material properties of the mushroom stipe are defined, assuming it to be an isotropic material. The parameters for elastic materials are set as shown in Table 2 of Section 2.2, including elastic modulus, yield stress, and Poisson's ratio. For the setting of viscoelastic parameters, Prony series is typically used for description [17], with the time domain selected. The parameters of the Prony series can be obtained by the conversion of the Maxwell model parameters. The expressions are as follows:

$$\bar{g}_i^p = \frac{E_i}{E_0} \tag{4}$$

$$\bar{g}_i^p = \bar{k}_i^p \tag{5}$$

$$\bar{\tau}_i^p = T_i \tag{6}$$

$$E_0 = E(t = 0) = E_\infty + \sum_{i=1}^{n} E_i \tag{7}$$

where $\bar{g}_i^p$ is the shear modulus, $\bar{\tau}_i^p$ is the relaxation time, and $\bar{k}_i^p$ is the bulk modulus.

According to Equation (3) in Section 2.3, the Maxwell model parameters for the mushroom stipe samples can be converted to the viscoelastic parameters of the mushroom stipes in the ABAQUS 2023 software, as shown in Table 3.

Table 3. The visco-elastic material parameters of stipe for FEA.

Materials	$\bar{g}_1^p$	$\bar{g}_2^p$	$\bar{\tau}_1^p$	$\bar{\tau}_2^p$
stipe	0.087672031	0.110973567	2.7445	27.15

The assembly drawings created by SolidWorks were imported into ABAQUS 2023 software. The mushroom stipes, the texture analyzer probe, and the metal plate were modeled as 3D solids. An important step in finite element analysis is "meshing", a process in which a 3D model is divided into smaller individuals. Such individuals are the basic elements of ABAQUS and are referred to as elements.

In agricultural fruit and vegetable simulation, hexahedral elements are usually used for meshing [20]. Hexahedral meshes have higher accuracy, fewer nodes, and lower computational cost than tetrahedral meshes, and are capable of handling plasticity, large deflections, and large strains. Moreover, they are also suitable for modeling irregular shapes and curved boundaries. Therefore, the mushroom stipes, the texture analyzer probe, and the metal plate were meshed with hexahedral cells. In contact stress analysis, the contact region is the most important. Compared with other regions, the contact region should have good mesh conformity. So, the meshing should create a denser mesh in the contact area between the mushroom stipe and the texture analyzer probe, as well as between the mushroom stipe and the metal plate. Additionally, it should be ensured that the integration points in the contact area can be corresponded. The meshing of the 3D model is shown in Figure 7.
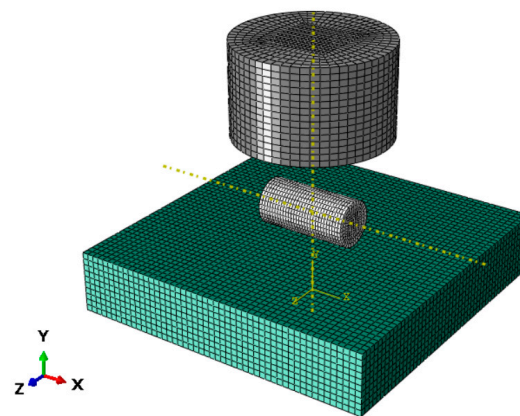

Figure 7. Finite element meshing of 3D model.

In the analysis step module, the stress relaxation process can be divided into two steps. First, the static general analysis step is selected to analyze the process of quasi-static compression. Second, the viscous analysis step is selected for analyzing the stress relaxation process. In the interaction module, the probe is set to be in contact with the mushroom stipe and the metal plate is set to be in contact with the surface of the stipe. Both sliding formulation are set to finite sliding, while the surface smoothing option is set to automatic smoothing of the 3D geometry surfaces when applicable. The normal behavior is set as hard contact, while the tangential behavior is set as having frictional contact. Additionally, in this finite element analysis, the main focus is on the deformation and stress change of the surface of the mushroom stipe, so the probe and the metal plate can be set as rigid bodies.

2.4.2. Finite Element Modeling Results and Discussion

After the pre-processing of the simulation operation was completed, the simulation scene was executed. The simulation results were obtained with effective data and visualization results. Stress relaxation simulation was carried out for mushrooms with stipe diameters of 10, 12, 14, and 16 mm, respectively, in which the stress relaxation simulation of mushroom stipes with a diameter of 16 mm is shown in Figure 8. The point of maximum contact stress on the mushroom stipe is the contact point between the stipe and the upper and lower plates. When the stress relaxation times were 0 s, 30 s, and 60 s, the maximum stresses of the mushroom stipe were 0.1230, 0.1042, and 0.1013 Mpa. The relaxation stresses decreased greatly in the first 10 s of relaxation time, then followed by a gradual and steady decline until reaching a balanced state. Moreover, the finite element analysis can obtain the

relaxation change of the pressure on the contact point of the mushroom stipe with time. The variation curve of the pressure with time on the mushroom stipe with a diameter of 16 mm is shown in Figure 9.
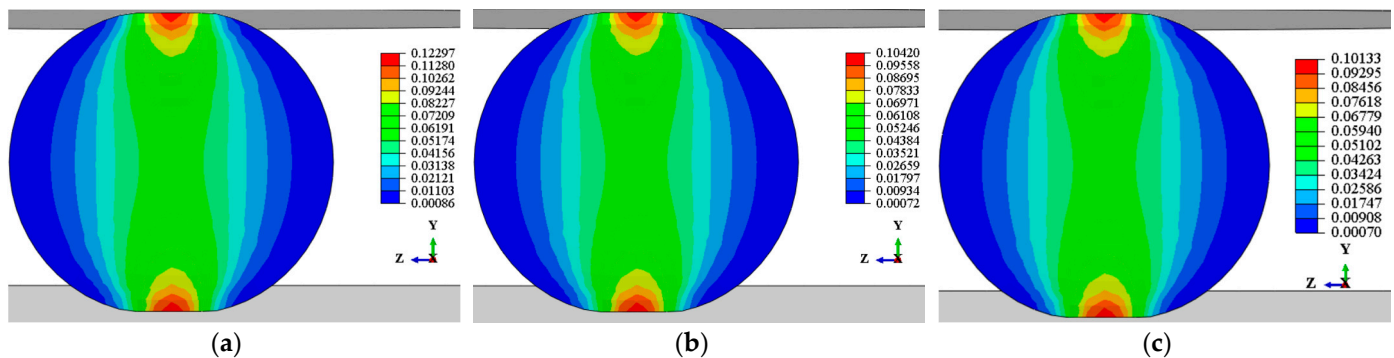
Figure 8. Variation of relaxation stress of mushroom stipes with time: (**a**) 0 s; (**b**) 30 s; (**c**) 60 s.
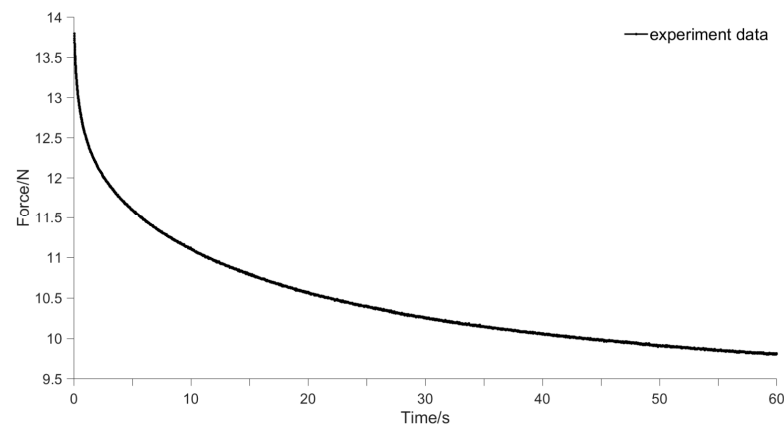
**Figure 9.** Variation of pressure on mushroom stipes with time.

3. Structure Design of Picking Grasper

The manual method of mushroom picking involves gripping the base of the stipe with the thumb and forefinger of one hand, rotating the stipe left and right, and slowly pulling it upward to detach it from the substrate. During harvesting, attention should also be paid to ensure that the hand can only touch the stipe, without causing any damage to the mushroom cap or gills. In view of this, the mushroom picking grasper designed in this paper, shown in Figure 10, features an integrated gripping and twisting structure. After successfully gripping the mushroom stipe with the fingers, the stipe is separated by a twisting motion at its base to achieve separation. Throughout the entire picking process, the fingers do not come into contact with the mushroom cap or gills.

The gripping actuator mainly includes finger, finger connector, supporting rod, sliding block, connecting rod, grooved cam, etc., as shown in Figure 11. In order to prevent damage to the mushroom cap during gripping, the finger is designed as an "L"-shaped structure, and made of TPU 95A material. The maximum distance between the fingers is 80 mm, which can effectively avoid contact with the cap. Each finger is equipped with a 1 mm thick silicone pad on the surface to increase friction between the finger and the fruit, ensuring stable gripping and preventing the stipe from slipping [21]. Three "L"-shaped fingers are evenly distributed at the base of the picking grasper, and their motion is roughly the same. The grooved cam adopts a centering structure, and is symmetrically distributed about the center of the mechanism; the whole is a triangular symmetrical structure, as shown in Figure 12. The connecting rod is connected to the sliding block, and by controlling the rotation angle and direction of the servo motor, it can move within the cam groove according to a predetermined pattern. This mechanism converts the rotational motion of
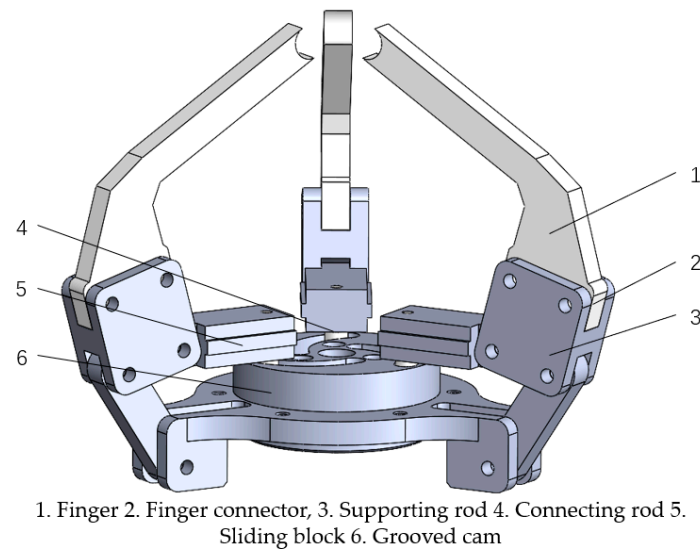
the servo motor into translational motion of the sliding block, causing the picking grasper to contract inward.
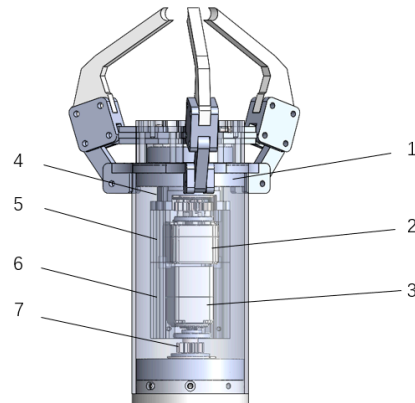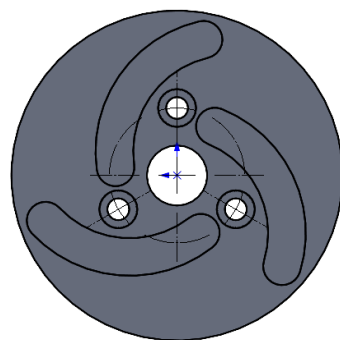

1. Bearing 2. Servo motor for clamping 3. Servo motor for rotating 4. Top fixing bracket 5. Servo fixing bracket 6. Servo fixing bracket 7. Clamping gear

Figure 10. The overall structure of the picking grasper.

1. Finger 2. Finger connector, 3. Supporting rod 4. Connecting rod 5. Sliding block 6. Grooved cam

Figure 11. The gripping actuator of the picking grasper.

Figure 12. The structural design of the grooved cam.

The rotating actuator mainly includes servo motor, clamping gear, servo fixing bracket, bottom fixing bracket, top fixing bracket, bearings, etc. The clamping gear remains stationary while the large gear meshes with it. The output shaft of the servo motor is connected to the big gear, driving it to rotate synchronously around the clamping gear. Meanwhile, to secure the servo motor, it is closely embedded with a servo fixing bracket. The servo fixing

bracket is embedded in a bearing, and the bearing is embedded in the top fixing bracket. The top fixing bracket is connected to the outer shell of the picking grasper. When the servo motor rotates, it drives the entire grasper to rotate, accordingly.

4. Kinematic Mechanics Analysis of the Grasper

4.1. Force Analysis of Gripping Actuator

In the gripping process of the grasper gripping actuator, the driving force starts from the servo motor, by transmitting through the grooved cam, connecting rod, sliding block, supporting rod, and TPU finger structure, and ultimately acting on the gripped mushroom stipe. Therefore, in order to obtain the gripping force of the finger acting on the mushroom stipe, it is necessary to carry out a static analysis of the gripping actuator and the finger structure. For the picking method of twisting the mushroom stipe, the relationship between the grasper's gripping force, twisting separation torque, and servo output torque is analyzed. Given the symmetric distribution of the three fingers relative to the groove cam, with identical structures, and the servo output torque acting at the center of the groove cam, the motion process and force situation are similar. Therefore, the analysis of the force exerted by the fingers on the mushroom stipe starts from a single finger, simplifying the analysis process.

The structure and motion principle of the grasper's gripping actuator are shown in Figure 13. The finger can be equated to a single concentrated force in the force analysis (the force and torque analysis on the finger structure is discussed below). During grasping, the servo motor drives the grooved cam to rotate clockwise, and the cam pulls the sliding block to move and drives the supporting rod to move. Subsequently, the finger connector is driven by the support rod to rotate around the joint FF to realize the gripping motion of the finger.
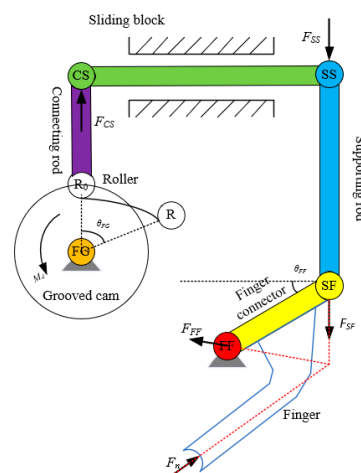
Figure 13. The motion schematic of grasper.

In the figure, M_d is the servo output torque; θ_{FG} is the angle between the initial and final positions of the roller relative to the center of the grooved cam, and θ_{FF} is the angle between the finger connector and the horizontal direction.

Due to the negligible mass of the individual moving parts in this transmission mechanism, the gravity and inertia forces during the grasper's movement can be disregarded.

Under static equilibrium conditions, a mechanical analysis of the transmission mechanism is conducted. In the initial state, the connecting rod and support rod are in a vertical position. As the grooved cam rotates, the angles of both rods change minimally, which can be ignored for simplification. The connecting rod is considered as a two-force member, and by analyzing the force acting on the sliding block, we obtain the following:

$$F_{CS} = F_{SS} \tag{8}$$

The direction is opposite, where F_{XY} is the force of member *X* on member *Y*. In order to simplify the analysis, the sliding friction of the sliding block on the grooved cam is negligible. Thus, the supporting rod is a two-force rod. Take the finger connector and finger to analyze the force and then according to the geometrical condition of the equilibrium of the plane convergent force system, a closed force triangle can be obtained. To ensure the force balance between finger connector and finger, the following can be obtained:

$$F_n \cdot \cos\gamma = F_{FF} \cdot \cos\beta \tag{9}$$

$$F_n \cdot \sin\gamma + F_{FF} \cdot \sin\beta = F_{SF} \tag{10}$$

where F_n is the force between the finger and the mushroom stipe, i.e., the finger gripping force; γ is the angle of F_n in the horizontal direction; β is the angle of F_{FF} in the horizontal direction. According to Equations (9) and (10), the following can be obtained:

$$F_n = \frac{1}{\sin\gamma + \cos\gamma \tan\beta} F_{SF} \tag{11}$$

where

$$\gamma = \alpha + \theta_{FF} \tag{12}$$

$$\tan\beta = \frac{h}{L\cos\theta_{FF}\sin^2(\alpha - \theta_{FF})} - \frac{1}{\tan(\alpha - \theta_{FF})} \tag{13}$$

and where *h* is the distance from the finger connector to the bottom of the finger in the initial state; α is the angle of the finger in the horizontal direction in the initial state; *L* is the length of the finger connector.

In order to obtain the relationship between the servo output torque M_d and the gripping force F_n, the grooved cam is force analyzed. The moment balance equation at joint FG is given as follows:

$$F_{CR}R \cdot \cos\theta_{FG} = M_d \tag{14}$$

According to the force characteristics of a two-force rod,

$$F_{CS} = F_{FS} = F_{SF} \tag{15}$$

where F_{FS} and F_{SF} are in opposite directions.

From Equations (11), (14) and (15), we can obtain the following:

$$F_n = \frac{1}{\sin\gamma + \cos\gamma \tan\beta} \cdot \frac{1}{R\cos\theta_{FG}} \cdot M_d \tag{16}$$

where *R* is the radius of the grooved cam.

### 4.2. Contact Force Analysis between Finger and Mushroom Stipe

To facilitate the calculation, the mushroom stipe is simplified as a regular cylinder. The picking grasper designed in this paper features a 3-finger uniformly distributed arrangement. Therefore, it is only necessary to analyze a single finger. Considering the picking method of the picking grasper, the simplified single finger on the mushroom stipe plane force model is shown in Figure 14.

The gripping force of the finger on the mushroom stipe is F_n, the unit is N/m, and the direction is pointing to the center of the circle. F_s is the static friction of the finger on the mushroom stipe, the unit is N/m, and the direction is perpendicular to the gripping force. When the finger twists the mushroom stipe, the static friction F_s provides the twisting force for the twisting separation torque *T*. According to the torque calculation formula, the relationship between the twisting separation torque *T* and the static friction F_s can be obtained as follows:

$$T = F_s \cdot r \tag{17}$$

where

$$F_s = \mu \cdot F_n \tag{18}$$
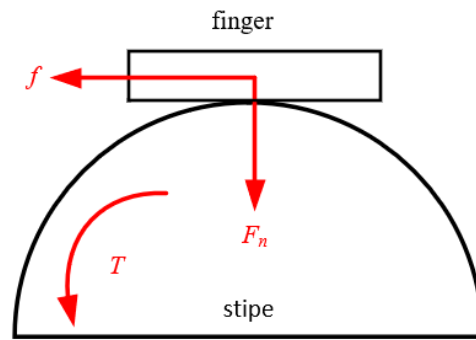
Figure 14. The plane force model of stipe.

In the equation, μ is the maximum static friction coefficient between the finger and the mushroom stipe; r is the radius of the mushroom stipe.

Therefore, from Equations (17) and (18), the relationship between the twisting separation torque T and the gripping force F_n can be obtained as below:
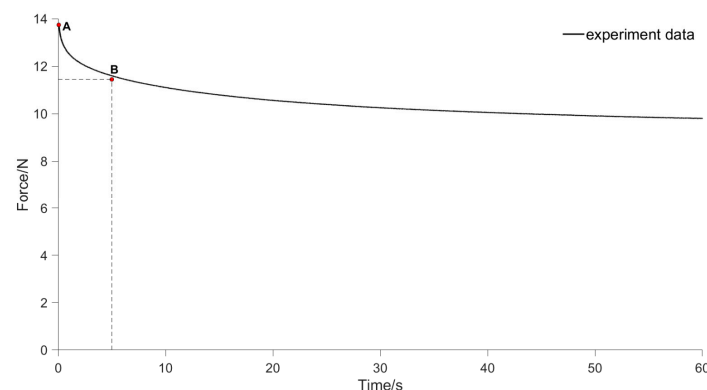
$$T = \mu F_n \cdot r \tag{19}$$

According to Equations (16) and (19), the relationship between the servo output torque M_d and the twisting separation torque T exerted by the finger on the mushroom stipe can be obtained as follows:

$$T = \frac{\mu r}{(\sin \gamma + \cos \gamma \tan \beta) \cdot R \cos \theta_{FG}} \cdot M_d \tag{20}$$

4.3. Grasper Picking Performance Analysis

The twisting separation torque required for picking mushrooms ranges from 0.092 N·m to 0.137 N·m. The larger the diameter of the mushroom stipe, the larger is the twisting separation torque T required, which is roughly linear. Additionally, the phenomenon of stress relaxation in the stipe needs to be considered. In the process of the grasper gripping and twisting the mushroom stipe, the displacement of the finger to the stipe remains constant, which belongs to the process of stress relaxation. The time required for the grasper twisting to separate the mushroom stipe is about 5 s, which is the stress relaxation time. The variation of pressure with time on the stipe with a diameter of 16 mm is shown in Figure 15. Point A is the pressure on the stipe in the initial state, and point B is the pressure on the stipe after 5 s. According to the stress relaxation equation of the stipe in Equation (3), the twisting separation torque required for the actual picking of shiitake mushrooms should be slightly larger than the twisting separation torque measured in the experiment, which is about 0.104 N·m to 0.155 N·m.

Figure 15. The pressure on the stipe decreases over relaxation time.

From Equations (16) and (20), the relationship between the grasper's gripping force F_n, twisting separation torque T of the fingers on the mushroom stipe, and the servo output

torque M_d is established. Therefore, when the twisting separation torque required for actual picking is determined, the corresponding servo output torque M_d can be obtained. At the same time, the gripping force F_n acting on the surface of the stipe can be determined. Considering the stress relaxation characteristics of the stipe during twisting, it should be circumvented to avoid that the clamping force F_n is greater than the maximum pressure that the stipe can withstand when twisting has just begun.

5. Test and Analysis

5.1. Verification Test of Stress Relaxation Properties of Mushroom Stipes

In order to validate the results of the finite element analysis of mushroom stipe stress relaxation discussed in Section 2.4, validation tests were conducted on the entire mushroom stipes. Four groups of stipes with diameters of 10, 12, 14, and 16 mm were used for the validation experiments, with each group comprising 10 stipes and a total of 40 samples. Due to the probe diameter of 50 mm, which is significantly larger than the stipe diameter, it is difficult to quantify accurately the contact area between the probe and the stipe. Therefore, it was difficult to calculate accurately the stress applied to the mushroom stipe when the validation tests were conducted on the whole stipe. As a result, we chose the parameter of pressure applied to the stipe to validate the results of the finite element analysis. The compression validation test was carried out on the sample with a compression deformation of 2 mm, compression rate of 1 mm/s, and the displacement was kept constant for 60 s. The pressure curve of the mushroom stipe was dynamically obtained by the texture analyzer, and the results were compared with those of the finite element analysis presented in Section 2.4. The results of the four groups of validation comparative tests are shown in Figure 16. The finite element analysis results exhibits a high degree of agreement with the experimental results, with a mean square error of less than 5%.
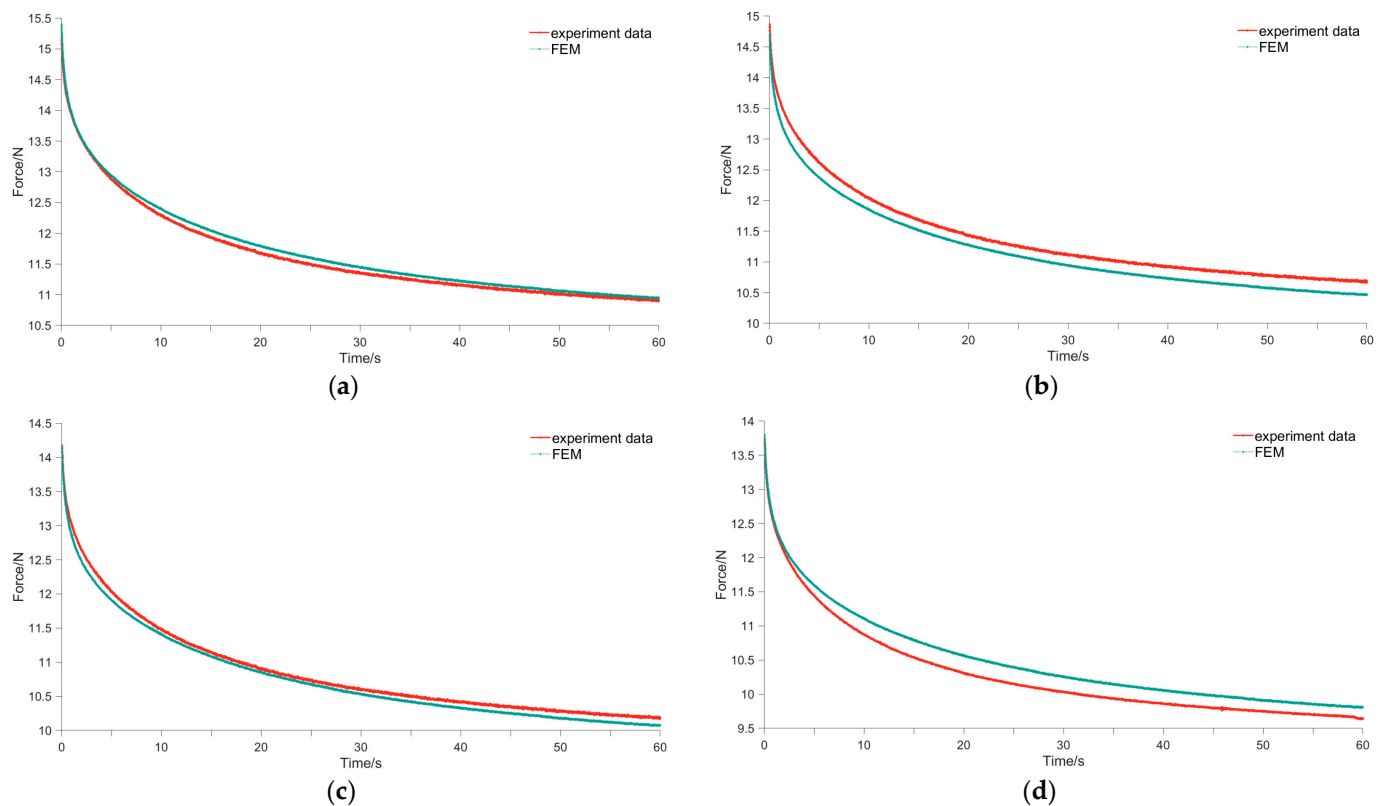
Figure 16. Comparison of the FEM results with the experimental results: (**a**) 10 mm; (**b**) 12 mm; (**c**) 14 mm; (**d**) 16 mm.

5.2. Test Analysis on the Picking Performance of the Picking Grasper

Under optimal conditions for mushroom cultivation, shiitake mushrooms typically take 4 to 10 days from bud formation to reach the harvesting standard. During this growth period, the cap diameter and stipe diameter of shiitake mushrooms vary. Therefore, shiitake buds with a cap diameter of approximately 1 cm were selected for subsequent experiments. The shiitake mushroom buds were selected after 4, 6, 8, and 10 days of growth under the same growth environment, resulting in four experimental groups. The number of shiitake mushrooms in each group was 20, and the total number of samples was 80. The average values of cap diameter and stipe diameter of shiitake mushrooms under different growth days are shown in Table 4. In order to validate the picking stability of the picking grasper designed in this paper, the picking grasper needed to be used to carry out mushroom picking tests on the above four groups of shiitake mushrooms.

Table 4. The stipe diameter and cap diameter of shii-take with different growing days.

Materials	4 Days	6 Days	8 Days	10 Days
Cap diameter (mm)	55.3	59.6	64.5	72.1
Stipe diameter (mm)	12.1	12.8	13.6	15.4

The experimental setup is shown in Figures 17 and 18. The picking grasper is fixed on the robotic arm (Franka), a seven-axis robotic arm with a high-sensitivity force-control performance, and the picking grasper is used to control the picking of mushrooms. In the test, the average time for the picking grasper to complete one picking cycle was 5.2 s. The actual picking success rate was observed and recorded, and the test results are shown in Table 5.

Figure 17. Contact model of picking grasper.

Figure 18. Structure diagram of the experimental device.

Table 5. The number of successful picks and the success rate of picking.

Days of Growth	Number of Successful Picks	Picking Success Rate
4	16	80%
6	18	90%
8	19	95%
10	15	75%

From the Table 5, it can be observed that the picking grasper designed in this paper demonstrates a high success rate of picking shiitake mushrooms with growth periods of 6 and 8 days, reaching 90% and 95%, respectively. Conversely, the success rate for mushrooms with growth periods of 4 and 10 days is relatively lower, at 80% and 75%, respectively. When the number of growth days of shiitake mushroom is 4 days, the average value of the stipe diameter is 12.1 mm, and when the number of growth days of shiitake mushroom is 10 days, the average value of the stipe diameter is 15.4 mm. The picking grasper designed in this paper is prone to finger slippage when gripping these two types of mushrooms, leading to a relatively lower success rate in picking. In addition, in order to compensate perfectly for the gripping force attenuation caused by the stress relaxation characteristics of the stipe, the grasper designed in this paper adopts stiff actuation. However, stiff actuation can cause plastic deformation to the stipe and may not envelope it well, which may also be a reason for the failure of picking. If a variable stiffness actuation is used, the displacement of the finger will change dynamically. At this time, the stress relaxation characteristics of the stipe are relatively complicated, and this will be the focus of our follow-up research. Therefore, the picking grasper designed in this paper is more effective for picking shiitake mushrooms with growth days of 6 to 8 days, cap diameters ranging from 59.6 mm to 64.5 mm, and stipe diameters between 12.8 mm and 13.6 mm. Additionally, this growth stage is also the most suitable stage for picking shiitake mushrooms.

6. Conclusions

To address the problem of non-destructive picking of shiitake mushrooms, the mechanical properties of shiitake mushroom picking were first analyzed. The compression mechanical test and stress relaxation test were carried out on mushroom stipe sections. The dynamic stress relaxation characteristics of mushroom stipes were then quantified by Maxwell's equation, yielding the final result: $E(t) = 0.02516e^{-t/2.7445} + 0.03088e^{-t/27.15} + 0.26196$. Subsequently, finite element simulation was employed to model the stress changes during stipe compression, combined with the above parameters. The pressure on the stipes obtained dynamically by the texture analyzer was verified with the finite element simulation results, while the mean square error between the simulation results and the actual results did not exceed 5%. Thus, the finite element simulation results were found to be satisfactory in comparison with the actual results.

Combined with the biological characteristics of the mushroom, a mushroom picking grasper was designed. The static analysis of the grasper's structural model was conducted, and the relationship between the grasper's gripping force, twisting separation torque, and servo output torque was obtained. Utilizing the dynamic stress relaxation properties of the stipes, the optimal twisting separation torque of the picking grasper for the shiitake mushroom and the corresponding output torque of the steering machine were calculated. For different diameters of mushroom stipes, the servo output torque was regulated to realize the optimal picking of the mushrooms. Additionally, tests were conducted on mushrooms of varying growth durations. The results show that the designed picking grasper is suitable for the automated non-destructive picking of shiitake mushrooms. It exhibits the best performance for shiitake mushrooms with growth days of 6 to 8 days, cap diameter of 59.6–64.5 mm, and stipe diameter of 12.8–13.6 mm.

References

1. Li, S.; Wang, A.; Liu, L.; Tian, G.; Wei, S.; Xu, F. Evaluation of nutritional values of shiitake mushroom (*Lentinus edodes*) stipes. *J. Food Meas. Charact.* **2018**, *12*, 2012–2019. [CrossRef]
2. Cefa. Analysis of the results of the 2021 national edible mushroom statistical survey. *Edible Fungi China* **2022**, *42*, 118–127.
3. Mu, L.; Cui, G.; Liu, Y.; Cui, Y.; Fu, L.; Gejima, Y. Design and simulation of an integrated end-effector for picking kiwifruit by robot. *Inform. Process. Agric.* **2020**, *7*, 58–71. [CrossRef]
4. Chen, K.; Li, T.; Yan, T.; Xie, F.; Feng, Q.; Zhu, Q.; Zhao, C. A soft gripper design for apple harvesting with force feedback and fruit slip detection. *Agriculture* **2022**, *12*, 1802. [CrossRef]
5. Bac, C.W.; Hemming, J.; Van Tuijl, B.A.J.; Barth, R.; Wais, E.; van Henten, E.J. Performance evaluation of a harvesting robot for sweet pepper. *J. Field Robot.* **2017**, *34*, 1123–1139. [CrossRef]
6. Xu, L.; Liu, X.; Zhang, K.; Yuan, Q.; Chen, J.; Yu, C. Design and test of end-effector for navel orange picking robot. *Trans. Chin. Soc. Agric. Eng.* **2018**, *34*, 53–61.
7. Reed, J. Initial experiments in robotic mushroom harvesting. *Mechatronics* **1994**, *4*, 265–279. [CrossRef]
8. Huang, M.; He, L.; Choi, D.; Pecchia, J.; Li, Y. Picking dynamic analysis for robotic harvesting of Agaricus bisporus mushrooms. *Comput. Electron. Agric.* **2021**, *185*, 106145. [CrossRef]
9. Lu, W.; Wang, P.; Wang, L.; Yiming, D. Design and experiment of flexible grip per for mushroom non-destructive picking. *Trans. Chin. Soc. Agric. Mach.* **2020**, *51*, 28–36.
10. Huang, M.; Yang, X.; Zhang, C.; Li, H.; Wu, H.; Wang, F. Study on harvesting dynamics of button mushroom and its picking end-effector design. *J. Chin. Agric. Mech.* **2023**, *44*, 66–70.
11. Ni, T.; Sun, X.; Li, D.; Zhao, Y.; Zhang, P.; Deng, Y. Compliance control strategy of parallel robot based on external force estimation. *Trans. Chin. Soc. Agric. Mach.* **2022**, *53*, 443–451.
12. Miao, Y.; Zheng, J. Development of compliant constant-force mechanism for end effector of apple picking robot. *Trans. Chin. Soc. Agric. Eng.* **2019**, *35*, 19–25.
13. Yuan, L.; Cheng, H. *Viscoelastic Viscoelasticity*, 1st ed.; China University of Mining and Technology Press: Beijing, China, 2020; pp. 154–196.
14. Nobile, D.; Chilo, M.; Mentana, S.; Baiano, A. Use of the generalized Maxwell model foidescribino the stress relaxation behavior of solid-like foods. *J. Food Eng.* **2007**, *78*, 978–983. [CrossRef]
15. Lu, H.; Ma, D.; Wang, J.; Yu, J. Research on mechanical behavior of viscoelastic food material inthe mode of compressed chewing. *Math. Probl. Eng.* **2015**, *2015*, 581424. [CrossRef]
16. Jiang, Z.; Chen, Y.; Tan, J.; Li, B.; Zou, X. Experimental Study on Stress Relaxation Characteristics and Associated Damage of Litchi. *Mod. Food Sci. Technol.* **2015**, *31*, 96–101.
17. Xia, X.; Xu, Z.; Yu, C.; Zhou, Q.; Chen, J. Finite Element Analysis and Experiment of the Bruise Behavior ofCarrot under Impact Loading. *Agriculture* **2021**, *11*, 471–480. [CrossRef]
18. Zou, L.; Yuan, J.; Liu, X.; Li, J.; Zhang, P.; Niu, Z. Burgers viscoelastic model-based variable stiffness design of compliant clamping mechanism for leafy greens harvesting. *Biosyst. Eng.* **2021**, *208*, 1–15. [CrossRef]
19. Mahiuddin, M.; Godhani, D.; Feng, L.; Liu, F.; Langrish, T.; Karim, M. Application of Caputo fractional rheological model to determine the viscoelastic and mechanical properties of fruit and vegetables. *Postharvest Biol. Technol.* **2020**, *163*, 111147. [CrossRef]
20. Ashtiani, S.; Sadrnia, H.; Mohammadinezhad, H.; Aghkhani, M. FEM-based simulation of the mechanical behavior of grapefruit under compressive loading. *Sci. Hortic.* **2019**, *245*, 39–46. [CrossRef]
21. Tang, Z.; Lu, J.; Wang, Z.; Ma, G. The development of a new variable stiffness soft gripper. *Int. J. Adv. Robot. Syst.* **2019**, *16*, 187–213. [CrossRef]